Published in : Geoderma(2013), 207, pp. 310--322.
doi:10.1016/j.geoderma.2013.05.024
Status : Postprint (Author's version)

CHARACTERIZATION OF TILLAGE EFFECTS ON THE SPATIAL VARIATION OF SOIL PROPERTIES USING GROUND-PENETRATING RADAR AND ELECTROMAGNETIC INDUCTION

François Jonard [a] , Mohammad Mahmoudzadeh [b], Christian Roisin [c], Lutz Weihermüller [a], Frédéric André [b], Julien Minet [b], Harry Vereecken [a], Sébastien Lambot [b]

[a] Agrosphere (IBG-3), Institute of Bio- and Geosciences, Forschungszentrum Jülich GmbH, 52425 Jülich, Germany

[b] Earth and Life Institute, Université catholique de Louvain, Croix du Sud 2 Box L7.05.02, 1348 Louvain-la-Neuve, Belgium

[c] Agriculture and Natural Environment Department, Walloon Agricultural Research Centre, rue du Bordia 4, 5030 Gembloux, Belgium

KEYWORDS: Soil tillage ; Ground-penetrating radar ; Electromagnetic induction ; Digital soil mapping ; Soil water content ; Soil resistance

ABSTRACT

Tillage practices influence physical, chemical, and biological soil properties, which also affect soil quality and consequently plant growth. In this study, the main objective was to evaluate the effects of different tillage practices on soil physical properties such as soil water content (SWC) by using geophysical methods, namely, ground-penetrating radar (GPR) and electromagnetic induction (EMI). Additional measurements such as soil sampling, capacitance probe, and soil penetrometer data were acquired as ground truths. The study was performed for three contrasting tillage practices, i.e., conventional tillage (CT), deep loosening tillage (DL), and reduced tillage (RT), applied on different plots of an agricultural field. The data showed that tillage influences soil resistance in shallow soil layers (deeper tillage decreases soil resistance), which could be partly seen in on-ground GPR data. In addition, reference SWC measurements (capacitance probes and soil sampling) were in fairly good agreement with the water content estimates from off-ground GPR. We also observed a tillage effect on shallow surface SWC, while deeper SWC seems to be unaffected by tillage. Mean surface SWC was significantly lower for CT compared to DL and RT, which was partly explained by lower pore connectivity between the topsoil and the deeper layers after conventional tillage. Moreover, the variance of the SWC within the conventional tillage plots was larger than within the other plots. This larger SWC variability could be explained by a greater soil heterogeneity induced by the plowing process. Overall, this study confirms the potential of GPR and EMI for the determination of soil physical properties at the field scale and for the assessment of agricultural management practices.

Published in : Geoderma(2013), 207, pp. 310--322.
doi:10.1016/j.geoderma.2013.05.024
Status : Postprint (Author's version)

1. Introduction

Agricultural management practices can affect soil physical, chemical, and biological properties with consequences for the movement of water, nutrients, and pollutants in the vadose zone, and for plant growth (Strudley et al., 2008). Alternative management practices such as conservation tillage or reduced tillage are encouraged to prevent environmental risks like soil erosion, flooding, and pesticide leaching in the groundwater. However, producers are reluctant to adopt these practices as their effects on soil and crop production are not yet well understood (Alletto et al., 2011). The impact of tillage practices on soil hydraulic properties (Ndiaye et al., 2007; Sauer et al., 1990; Schwen et al., 2011a,b; Strudley et al., 2008) and their consequences on preferential flow (Elliott et al., 2000; Kulasekera et al., 2011), soil state variables (soil water content and soil temperature) (Kovar et al., 1992; Tan et al., 2002), soil physical properties (soil penetration resistance, soil bulk density, soil porosity) (Jabro et al., 2009), and plant growth (Alletto et al., 2011; Zhang et al., 2011) have been subject to intensive research over the past decade. However, according to the recent review by Strudley et al. (2008), experimental results from field and laboratory studies do not show consistent effects of tillage practices on soil properties. Moreover, to obtain information about soil properties, most of these studies used invasive methods such as time-domain reflectometry, capacitance sensors, or soil sampling, which are time-consuming and offer only local information. Therefore, these techniques are limited to a small spatial extent. In addition, time-lapse measurements are not feasible within agricultural fields, although they would provide valuable insights into the changes of the state variables (e.g., soil water content and soil temperature) or the processes involved.

In that respect, ground-penetrating radar (GPR) and electromagnetic induction (EMI) are non-invasive geophysical techniques which can be used to characterize the shallow subsurface properties at the field scale with high temporal and spatial resolutions (André et al., 2012; Cockx et al., 2007; Huisman et al., 2003; Jonard et al., 2011; Lambot et al., 2008; Slob et al., 2010). EMI is sensitive to soil electrical conductivity, which is mainly affected by soil water content (SWC), clay content, and salinity (Corwin and Lesch, 2005; Friedman, 2005), while GPR is sensitive to both soil electrical conductivity and dielectric permittivity, the latter primarily depending on SWC (Topp et al., 1980). Yet, until now, very few studies have used geophysical techniques to investigate the impact of tillage practices (e.g., Basso et al., 2011; Oleschko et al., 2008; Richard et al., 2010). Recently, Müller et al. (2009) compared different geophysical techniques to characterize tillage effects on SWC and electrical resistivity. However, their sampling scheme was limited to two transects, which did not permit them to fully explain their observations. Basso et al. (2011) used electrical resistivity tomography applied to an entire field area, which enabled them to study the spatiotemporal dynamics of soil physical properties. Nevertheless, a high resolution could not be achieved, especially at the soil surface.

The general objective of this present study is to analyze the effects of tillage practices on the spatial variation of soil properties by using geophysical techniques. In particular, we focused on surface SWC, bulk soil electrical conductivity, and mechanical resistance. The study was conducted on an agricultural field in the loess belt of central Belgium (Gentinnes). GPR and EMI measurements were performed for three contrasting tillage practices, i.e., conventional tillage (CT), deep loosening tillage (DL), and reduced tillage (RT). In this paper, we first present on-ground GPR images and soil strength maps to

Published in : Geoderma(2013), 207, pp. 310--322.
doi:10.1016/j.geoderma.2013.05.024
Status : Postprint (Author's version)

characterize the tillage effect on soil penetration resistance. Soil electrical conductivity and SWC maps from EMI and off-ground GPR data, respectively, are then presented and interpreted in the light of in situ observations. Finally, the tillage effect on SWC and its spatial distribution is discussed.

2. Materials and methods

2.1. EXPERIMENTAL SITE

The study was conducted on an agricultural field in Gentinnes, located in the loess belt of central Belgium (50°35′ N 4°35′ E). The soil is a silty loam soil classified as an Orthic Luvisol according to the FAO classification. Elevation varies between 137 and 145 m above sea level. The silt fraction dominates the clay and sand fractions (20.0, 74.5, and 5.5% for clay, silt, and sand, respectively) in the topsoil (0–25 cm), and the organic carbon content was 8.67 g kg^{-1}. The exact water table depth is unknown, but is in general deeper than 2 m. Since fall 2005, a soil tillage experiment has been implemented on the field to compare three contrasting tillage systems: (1) conventional tillage (CT) with moldboard plowing to ≈27 cm depth, (2) deep loosening tillage (DL) with a heavy tine cultivator to ≈30 cm depth, and (3) reduced tillage (RT) with a spring tine cultivator to ≈ 10 cm depth. The field was divided into 20 plots of 30 × 18 m^2 and each plot was characterized by one of the three tillage systems (Fig. 1). Only 12 plots were used for the geophysical measurements (4 replications per tillage system) and 3 other plots were used for the soil strength measurements. These 3 plots were located next to the 12 other plots, at a distance of about 15 m in the south-western part of the field (not shown in Fig. 1). The geophysical measurements were performed on April 13, 2010, while the soil strength measurements were performed on April 27, 2010. Average monthly rainfall recorded at a meteorological station located about 7 km away from the field was 75.3 mm in February, 36.0 mm in March, and 23.4 mm in April 2010. No rain was observed during the two measurement days and the daily reference evapotranspiration was close to 3 mm for both dates (Fig. 2).

2.2. AGRICULTURAL PRACTICES

Initially, the study site had been plowed in its entirety for several decades. Since 2005, it has been divided according to three tillage systems (CT, DL, and RT) and the same tillage treatment has been applied every year to the same plot, except in 2006 and 2008, where the DL tillage system was replaced by the RT tillage system. In 2006 and 2008, sugar beet was planted in April after seed bed preparation (with rotary harrow and drill), while winter wheat was sown in November (also with rotary harrow and drill). The wheat straw was chopped during the harvest and then mixed into the top soil layer by stubble harrowing. White mustard was used as a cover crop for all the plots during three fallow periods (2005–2006, 2007–2008, 2009–2010), i.e., before sugar beet planting. White mustard was always sown in September using rotary harrow and drill. The three tillage treatments (CT, DL, and RT) were systematically applied before sowing white mustard or winter wheat. In April 2010, one day before the geophysical measurements, a minimum tillage was applied to all the plots with a disk harrow (to a depth of 5 cm) in order to reduce soil surface roughness for the radar measurements (Jonard et al., 2012). The

Published in : Geoderma(2013), 207, pp. 310--322.
doi:10.1016/j.geoderma.2013.05.024
Status : Postprint (Author's version)

day after the geophysical measurements, the whole field was prepared for seed bed with a disk harrow (to a depth of 3 cm) and flax was sown.

2.3. REFERENCE SOIL WATER CONTENT MEASUREMENTS

Undisturbed soil samples (100 cm^3 Kopecky rings) were used as reference measurements for the volumetric SWC. Soil samples were collected between 0 and 5 cm depth on a regular grid in each plot (5 × 3 m spacing, i.e., 35 samples per plot and 420 samples in total). Soil samples were also taken at two locations in each plot between 0 and 75 cm depth in 5 cm steps. The two locations were chosen arbitrarily around the middle of each plot. The volumetric water content of the soil samples was obtained by the weight loss after oven drying at 105 °C for at least 48 h. At each sampling point, soil dielectric permittivity was measured using two capacitance sensors, namely, the ThetaProbe ML2x sensor (Delta-T Devices Ltd, Cambridge, UK) and the 5TE sensor (Decagon Devices Inc., Pullman, Washington, USA), which were inserted vertically into the soil. The ThetaProbe sensor operates at 100 MHz and has four stainless steel rods of 6 cm length while the 5TE probe operates at a frequency of 70 MHz and has 3 prongs of 5.2 cm length. Three measurements with each probe were performed at a distance of less than 15 cm around each sampling point. The soil water content was then determined from the soil dielectric permittivity using Topp's model (Topp et al., 1980). It should be noted that using a sitespecific relationship or a dielectric mixing model instead of Topp's model is likely to provide better absolute results. Nevertheless, Topp's model was chosen due to its simple application and because the present study is mainly focused on the comparison of SWC values with respect to different tillage treatments, which means that relative differences can be used.

2.4. GEOPHYSICAL MEASUREMENTS

2.4.1. GROUND-PENETRATING RADARS

Two different ground-penetrating radar (GPR) systems were used in this study: (1) off-ground radar for SWC retrieval and (2) common on-ground radar for soil stratigraphy imaging, whereby both radar systems were set up on an all-terrain vehicle (ATV) (Fig. 3).

2.4.1.1. Off-ground GPR. The radar system was set up using a ZVL vector network analyzer (VNA, Rohde & Schwarz, Munich, Germany), thereby providing an ultrawideband (UWB) stepped-frequency continuous-wave (SFCW) radar. The antenna system consisted of a transverse electromagnetic (TEM), double-ridged broadband horn antenna (BBHA 9120 F, Schwarzbeck Mess-Elektronik, Schönau, Germany). The antenna was 95 cm long with a 68 × 96 cm^2 aperture area and a - 3 dB full beamwidth in the E-plane and the H-plane of 46° (at 400 MHz). The antenna nominal frequency range was 0.2–2 GHz and its isotropic gain ranged from 9 to 14 dBi.

With this radar system, the raw data consist of the frequencydependent complex ratio S11 between the backscattered electromagnetic field (b(ω)) and the incident electromagnetic field (a(ω)), with ω being the angular frequency. The raw GPR data were obtained sequentially at 301 stepped operating frequencies over the range 0.2–2 GHz with a frequency step of 6 MHz. Only lower frequency data (0.2–0.4 GHz), which were not affected by soil surface roughness, were used for the inversions. Assuming that

Published in : Geoderma(2013), 207, pp. 310--322.
doi:10.1016/j.geoderma.2013.05.024
Status : Postprint (Author's version)

the distribution of the electromagnetic field measured by the antenna is independent of the scatterer, i.e., only the phase and amplitude of the field change (plane wave approximation over the antenna aperture), the following radar equation applies (Lambot et al., 2004):

$$S_{11}(\omega) = \frac{b(\omega)}{a(\omega)} = H_i(\omega) + \frac{H(\omega)\hat{G}_{xx}(\omega)}{1 - H_f(\omega)\hat{G}_{xx}(\omega)} \quad (1)$$

where $H_i(\omega)$ is the antenna return loss, $H(\omega)$ is the antenna transmitting– receiving transfer function, $H_f(\omega)$ is the antenna feedback loss, and $G^{\uparrow}_{xx}(\omega)$ is the transfer Green's function of the air–soil system. The Green's function represents a solution of the 3D Maxwell equations for electromagnetic waves propagating in multilayered media (Michalski and Mosig, 1997).

In order to identify the surface dielectric permittivity, inversion of the Green's function is performed in the time domain, focusing on a time window containing the surface reflection only (Lambot et al., 2006). The inverse problem is formulated in the least-squares sense and the objective function to be minimized is defined accordingly as follows:

$$\phi(\mathbf{b}) = \left(\mathbf{g}^{\uparrow *}_{xx} - \mathbf{g}^{\uparrow}_{xx}\right)^T \cdot \left(\mathbf{g}^{\uparrow *}_{xx} - \mathbf{g}^{\uparrow}_{xx}\right) \quad (2)$$

where

$$\mathbf{g}^{\uparrow *}_{xx} = g^{\uparrow *}_{xx}(t)\big|_{t_{min}}^{t_{max}} \quad \text{and} \quad \mathbf{g}^{\uparrow}_{xx} = g^{\uparrow}_{xx}(t)\big|_{t_{min}}^{t_{max}} \quad (3)$$

are the vectors containing, respectively, the observed and simulated time-domain windowed Green's functions, and b = [εr,ha] is the parameter vector to be estimated, with ε_r [dimensionless] being the soil surface relative dielectric permittivity and ha [m] being the distance between the antenna phase center and the soil surface. As for the capacitance water content sensors, the water content was derived from the dielectric permittivity using Topp's model.

2.4.1.2. On-ground GPR. We used a time-domain GPR system (model SIR-20, Geophysical Survey Systems, Inc., Salem, Massachusetts, USA) combined with a transmitting (Tx) and receiving (Rx) 400 MHz center-frequency-shielded bowtie antenna with a Tx and Rx offset of 0.16 m. GPR data were collected with a sampling interval of 5 cm, and 512 samples per scan were recorded with 16 bits per sample. The GPR produces a Ricker-type pulse with a frequency bandwidth of 100–800 MHz. The gain function was enabled at 5 points in order to highlight deeper reflections. The time window was limited to 50 ns. The on-ground GPR was used for soil imaging only (data were not inverted). It is worth noting that we did not use the data from the bistatic radar configuration (1.10 m Tx–Rx offset) shown in Fig. 3.

Fig. 1. *Study site at Gentinnes, Belgium. Sampling points for the reference measurements and the off-ground GPR data acquisition are shown. The location of the three selected on-ground GPR transects (see Fig. 6) is also shown. Background colors represent the three tillage systems: conventional tillage, deep loosening tillage, and reduced tillage.*

Published in : Geoderma(2013), 207, pp. 310--322.
doi:10.1016/j.geoderma.2013.05.024
Status : Postprint (Author's version)

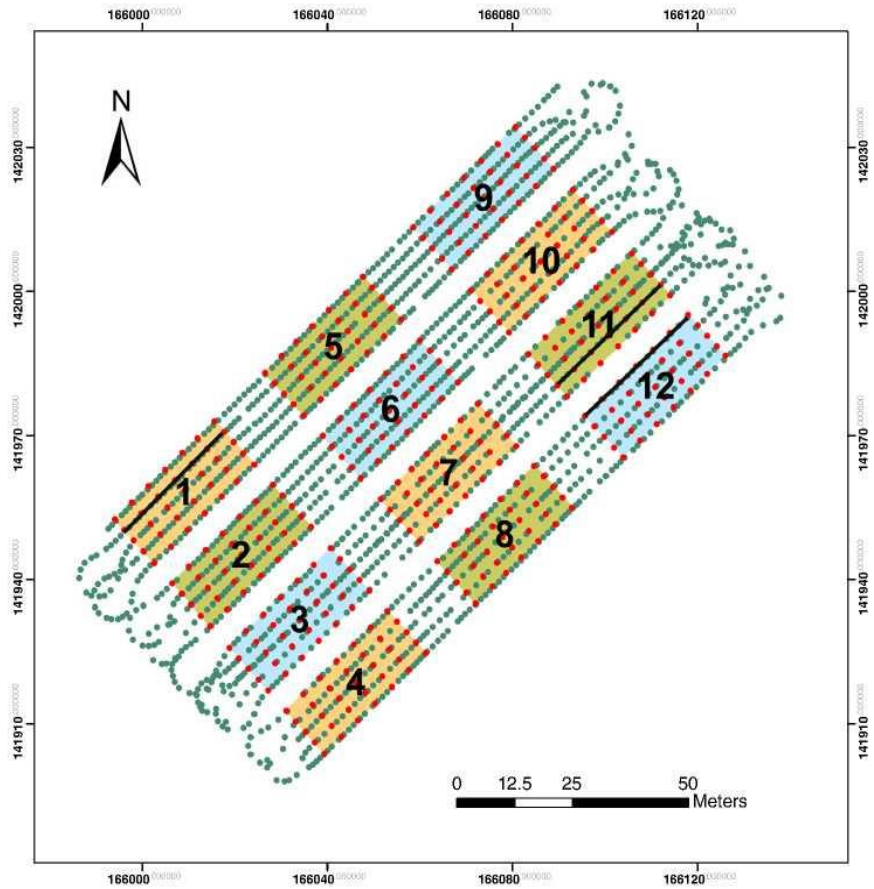

Experimental Setup

Tillage systems

- Conventional Tillage
- Deep Loosening Tillage
- Reduced Tillage

- **Ground-truth data**
- **Off-ground GPR data**
- **On-ground GPR transects**

Projected Coordinate System: Belgian Lambert 1972
Projection: Lambert Conformal Conic
Ellipsoid : Hayford 1924
Datum: Belgian Datum 1972

Published in : Journal (année), vol. xx, n°xx, pp. xx–xx
DOI:xxxxxxxxxxxxxx
Status : Postprint (Author's version)

Fig. 2. *Daily rainfall (P) and daily reference evapotranspiration (ETo) in mm measured at the Ernage–Gembloux weather station during April 2010. Arrows indicate the first (A) and second (B) measurement day.*

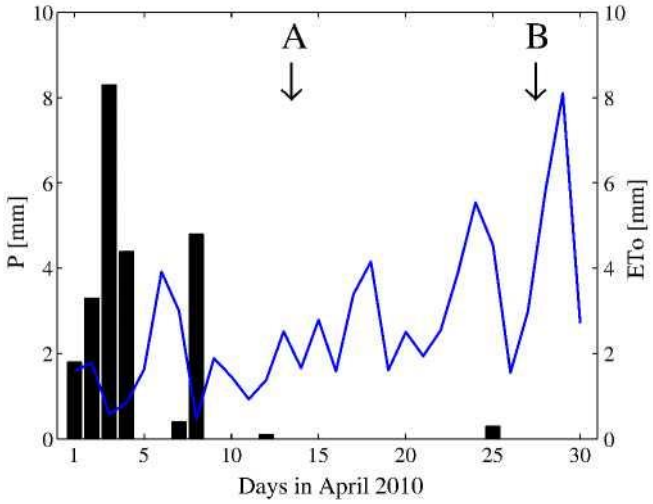

Fig. 3*. Off-ground GPR (horn antenna linked to a vector network analyzer, DGPS device, and a PC), on-ground GPR, and the EM38 sensor mounted on an all-terrain vehicle as well as the Profiler sensor carried manually.*

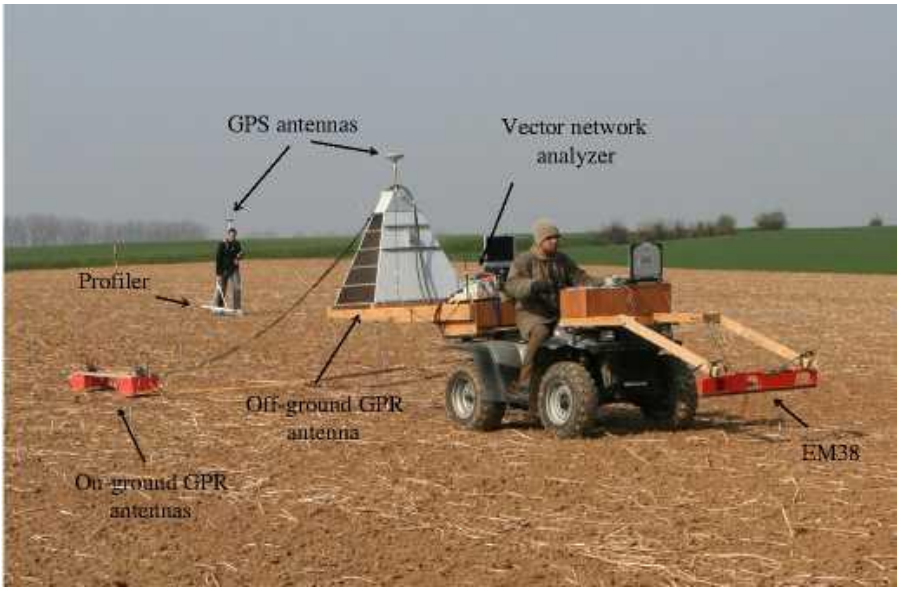

2.4.2. ELECTROMAGNETIC INDUCTION

EMI data were acquired with the Profiler EMP-400 (Geophysical Survey Systems, Inc., Salem, Massachusetts, USA) and the EM38 (Geonics Limited, Mississauga, Ontario, Canada) sensors. The Profiler was manually carried at about 0.10 m above the ground surface and allowed to perform

Published in : Journal (année), vol. xx, n°xx, pp. xx–xx
DOI:xxxxxxxxxxxxxx
Status : Postprint (Author's version)

measurements simultaneously at three different frequencies: 5, 10, and 15 kHz. The data were recorded every second, corresponding to an average sampling interval of about 0.80 m. In contrast, the EM38 was mounted on the front of the ATV at about 0.30 m above the ground surface (see Fig. 3) and the data were recorded at one frequency only (14.7 kHz). The EM38 was fixed at a sufficient distance (about 1.30 m) from the ATV to avoid interferences. Profiler data were collected with both horizontal and vertical dipole orientations, while EM38 measurements were performed with vertical dipole orientation only. The use of different frequencies and dipole orientations permitted different soil depths to be investigated. All equipment (GPR and EMI sensors) was georeferenced by means of a differential global positioning system (DGPS).

2.5. SOIL STRENGTH MEASUREMENTS

The soil strength measurements were performed in three plots characterized by the three tillage methods and located next to the twelve plots previously investigated. These measurements were performed two weeks after the geophysical measurements. A fully automated penetrometer (30° angle cone with a base area of 1 cm^2) mounted on a small vehicle was used as described by Roisin (2007) (Fig. 4). Two areas of 80 × 80 cm^2 located side by side were investigated. These two squares were divided along a 16 × 16 lattice (with 5 cm spacing between neighboring points) yielding a total of 256 nodes each. At each node, a penetration was performed, and data were collected every centimeter from the surface down to a depth of 45 cm. This procedure resulted in a 32 × 32 matrix of resistance values at each of 45 depth levels.

2.6. STATISTICAL ANALYSIS

A linear mixed model was used to test for the effects of tillage treatment and sensor on the soil volumetric water content (θ [m^3 m^{-3}]):

$$\theta_{ijk} = \mu + \alpha_i + \beta_j + \gamma_{ij} + \varepsilon_{ijk} \qquad (4)$$

where μ is the total mean θ, αi is the sensor effect with i levels (i =1 for ThetaProbe, 2 for 5TE, 3 for soil sampling, and 4 for off-ground GPR), βj is the tillage effect with j levels (j = 1 for CT, 2 for DL, and 3 for RT), γij is the interaction term between sensor and tillage, and εijk is the residual term for the kth observation of the ith and jth sensor and tillage levels, respectively.

A linear mixed model was also used to test for the effects of tillage treatment, sensor, and sensor operating frequency on the soil apparent electrical conductivity (σ [mS m^{-1}]):

$$\sigma_{ijke} = \mu + \alpha_i + \beta_j + \gamma_k + \delta_{ij} + \zeta_{ik} + \eta_{jk} + \nu_{ijk} + \varepsilon_{ijke} \qquad (5)$$

where μ is the total mean σ, α_i is the sensor effect with i levels (i =1 for EM38, 2 for Profiler with horizontal dipoles, and 3 for Profiler with vertical dipoles), βj is the frequency effect with j levels (j = 1 for 5 kHz, 2 for 10 kHz, 3 for 15 kHz, and 4 for 14.7 kHz), γ_k is the tillage effect with k levels (k = 1 for

Published in : Journal (année), vol. xx, n°xx, pp. xx–xx
DOI:xxxxxxxxxxxxxxx
Status : Postprint (Author's version)

CT, 2 for DL, and 3 for RT), δij is the interaction term between sensor and frequency, ζ_{ik} is the interaction term between sensor and tillage, ηjk is the interaction term between frequency and tillage, v_{ijk} is the triple interaction term, and ε_{ijke} is the residual term for the eth observation of the ith sensor level, the jth frequency level, and the kth tillage level.

In these models, α, β, γ, δ, ζ, η, and ν were considered as linear fixed effects and the spatial correlation among the data was taken into account by considering a covariance pattern with an exponential structure for the residuals (Brown and Prescott, 2006). The models were fitted using the MIXED procedure of the SAS software (Version 9.3; SAS Institute Inc., Cary, North Carolina, USA). The fitted models were selected on the basis of the Akaike information criterion (AIC). Weak collinearity between independent variables was checked, as were residual homoscedasticity and residual normal distribution. Contrasts were used to test the differences between tillage treatments for a given sensor (Eq. (4)) or for a given sensor and frequency (Eq. (5)). All statistical tests were performed at a 0.05 significance level.

3. Results and discussion

3.1. SHALLOW SOIL STRATIGRAPHY IMAGING

First, we analyzed the shallow soil stratigraphy using the 2D soil strength maps as depicted in Fig. 5 obtained by the penetrometer for the three different tillage systems (CT, DL, and RT). It should be noted that the 2D vertical profiles were calculated by averaging the data collected in 3D over one direction (y-axis) for better visualization. In all cases, the profiles are depicted in the perpendicular direction of the tillage practice to highlight the tillage effect on soil resistance. Fig. 5a clearly shows two distinct layers for the CT, whereby the first layer (0–25 cm depth) is characterized by lower resistance values (b 2.5 MPa) compared to the second layer with resistance values exceeding 2.5 MPa. The lower resistance value of the first layer can be explained by the plowing, which generally reduces soil compaction in the top layer. In general, the resistance of the first layer is quite homogeneous, but on the top left (between the distances of 20 and 80 cm) two blocks with higher resistance can be observed which correspond to areas of compaction below the tractor tracks. The second layer with generally higher compaction values indicates a clear stratigraphic increase of resistance with depth. The DL map (Fig. 5b) also shows two distinct layers, but with less clear separation and greater heterogeneity. The uneven separation of the layering can also be explained by the tillage practice, whereby the two main prongs of the heavy tine cultivator caused the local changes during the deep loosening. Nevertheless, a layer separation can be detected between 20 and 25 cm depth. In comparison to CT and DL, RT (Fig. 5c) shows a much finer top layer (about 10 cm depth), which can be related to the smaller penetration depth of the tine cultivator used for the reduced tillage. Additionally, the top layer is highly homogeneous. The irregularities observed in the second layer at about 20 cm depth can be attributed to previous tillage practices before 2005. These irregularities are not visible in the CT and DL plots because the plowing and deep loosening are both below 20 cm depth. In general, the penetrometer can be used to clearly distinguish the different

Published in : Journal (année), vol. xx, n°xx, pp. xx–xx
DOI:xxxxxxxxxxxxxxx
Status : Postprint (Author's version)

tillage practices and their effects on soil strength, but due to the time-consuming data acquisition (about 4 h for a volume of 80 × 160 × 45 cm^3) only a small area (or volume) can be sampled.

On the other hand, on-ground GPR allows non-invasive data acquisition over large areas within a relatively short time. As an example, Fig. 6 shows selected radargrams for the three tillage practices. Each radargram corresponds to a transect of one plot in the tillage direction (see Fig. 1 for the location of the selected transects). Although differences could be observed from a structural point of view, comparable results were obtained between the different transects within one tillage practice (results not shown). In general, all transects show a clear reflection at 4 ns corresponding to the antennas and antenna– soil couplings as well as a clear reflection at 9–10 ns indicating the interface between the disturbed surface layer and deeper soil. In the case of CT (Fig. 6a), a deeper soil layer at 14–15 ns can also be clearly observed, which corresponds to a sharp transition between two different horizons. However, this layer is less clearly visible for DL and RT. For RT plotted in Fig. 6c, the first interface becomes much clearer, which may be attributed to the shallower interface and greater contrast between the loose and compacted soil layers. In addition to the major reflections at the interface between tilled and non-tilled soil layers, local heterogeneities can be observed at greater depths (>20 ns), which may be caused by the presence of stones, or variations of local water content due to textural changes.

In the next step, we calculated the actual depth of the reflectors using the travel times and the dielectric permittivity averaged for the first layer obtained from the SWC information. Therefore, we averaged all water content data collected in all plots with the same tillage treatment from ThetaProbe readings (θ = 0.23, 0.26, and 0.27 $m^3\ m^{-3}$ for CT, DL, and RT, respectively). It is worth noting that some uncertainty is introduced by this procedure because only the mean surface SWC for each tillage treatment is used for each point in space. A more accurate estimation of the actual depths would have required knowledge of the detailed permittivity profiles. This is not straightforward given the inherent local variability. However, the scope of this analysis is only to provide insights with respect to the depth of the reflectors, specifically to compare the three tillage practices. The second reflection observed at 9–10 ns is likely to result from shallow density changes (depths of about 22 cm for CT, 20 cm for DL, and 19 cm for RT) due to the different tillage practices, which is in good agreement with the penetrometer maps. The third reflection occurring at 14–15 ns in the CT plots is attributed to the presence ofa more compacted soil layer below a depth of about 40–45 cm. It is worth noting that the interpretation of the radargrams with respect to the tillage practices is hampered by the relatively low depth resolution obtained by the 400 MHz antenna used ($\lambda/4 \approx 5$ cm, assuming a mean SWC of 0.25 $m^3\ m^{-3}$). In conclusion, on-ground GPR seems to be a helpful tool for real-time imaging of larger areas with respect to identifying shallow soil layers induced by different tillage practices. As shown, significant differences can already be observed between the different treatments, whereby better results would be obtained using higher frequencies to provide higher range resolution.

Fig. 4. *Fully automated penetrometer used for the soil strength measurements.*

Published in : Journal (année), vol. xx, n°xx, pp. xx–xx
DOI:xxxxxxxxxxxxxx
Status : Postprint (Author's version)

Fig. 5. *2D soil strength maps obtained by the penetrometer after (a) conventional tillage, (b) deep loosening tillage, and (c) reduced tillage.*

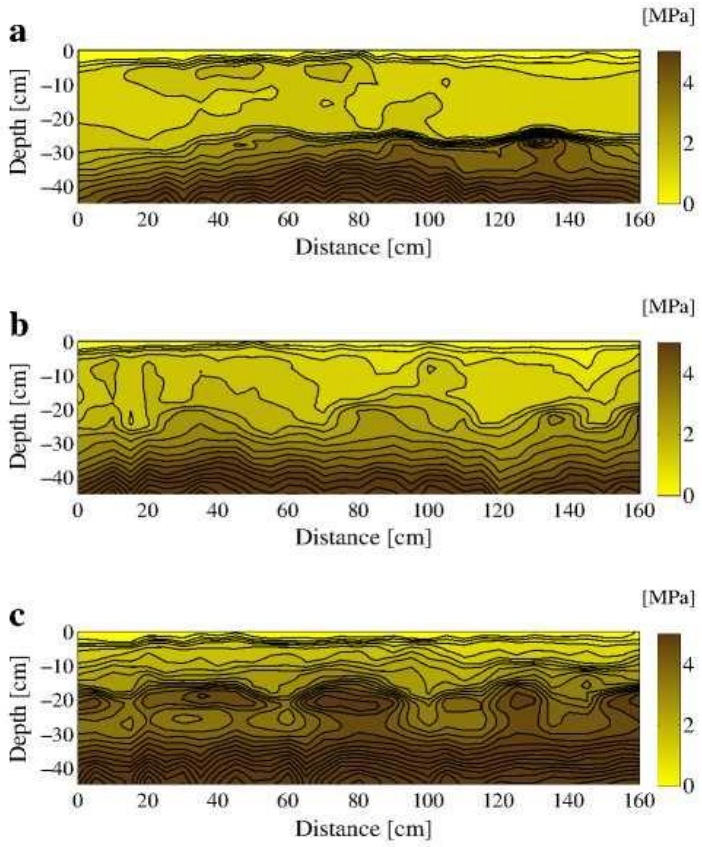

3.2. APPARENT SOIL ELECTRICAL CONDUCTIVITY

Apparent soil electrical conductivity (ECa) mainly depends on soil clay content, SWC, soil salinity, soil temperature, and, indirectly, on soil compaction due to changes in SWC (Corwin and Lesch, 2005; Friedman, 2005). As already stated, two different EMI sensors (Profiler and EM38) were used to map the apparent soil electrical conductivity to provide insights into the spatial variability of the soil

Published in : Journal (année), vol. xx, n°xx, pp. xx–xx
DOI:xxxxxxxxxxxxxxx
Status : Postprint (Author's version)

properties within the root zone. In general, EMI sensors measure a depth- weighted average of the electrical conductivity, referred to as apparent electrical conductivity (ECa). Fig. 7 shows ECa maps retrieved by the Profiler and the EM38 sensors. Fig. 7a and b were obtained from the Profiler operating with horizontal and vertical dipoles, respectively, at a frequency of 15 kHz and with a coil separation of 1.22 m. Fig. 7c was obtained from the EM38 at 14.7 kHz with vertical dipoles and a coil separation of 1 m. The different dipole orientations and coil separations provide different nominal depths of investigation, defined as the depth to which approximately 70% of the measured response is generated. For the Profiler, the nominal depth of investigation is 1.9 m and 0.9 m when operated in the vertical and horizontal modes, respectively, while the nominal depth of investigation of the EM38 is 1.6 m for the vertical dipole orientation (McNeill, 1980; Reedy and Scanlon, 2003). At lower frequencies (5 and 10 kHz), the nominal depth of investigation of the Profiler is expected to be slightly increased depending also on the soil electrical properties (Mester et al., 2011). The EM38 data were collected in one direction only while the Profiler data were collected in two perpendicular directions.

In general, a declining trend in ECa from the lower left to the upper right corner (from south to north) can be observed (Fig. 7), whereby this trend is independent of the underlying soil tillage practice of the different plots. This suggests that the tillage does not significantly affect the deeper SWC. For the entire field, ECa varies between 10 and 30 mS m^{-1}, which is a relatively small range of variation for agricultural fields (Brosten et al., 2011). This small variability of the EMI-derived EC_a can be explained by the small variability of clay content over the entire field (15.8–22.7 mass %). The EC_a derived from the vertical dipole orientation of the Profiler shows significantly higher values compared to the horizontal dipole measurements, which indicates an increase of ECa with depth. Indeed, the sensitivity of the measurements in horizontal dipole orientation is mostly affected by EC_a changes within the near-surface layer (b 0.40 m), whereas the vertical dipole mode shows a maximum sensitivity at deeper layers (0.8–1.0 m) (McNeill, 1980). On the other hand, the EM38-derived ECa map is relatively similar to the Profiler map measured at vertical dipole orientation, which is expected as both instruments operate at similar frequencies (15 kHz and 14.7 kHz) and with the same dipole orientation. Unfortunately, the two measurements (Profiler and EM38) were not performed at exactly the same location because the EM38 was mounted on the ATV and the Profiler was carried manually (see Fig. 3), and therefore, a straightforward comparison was not possible. To overcome this drawback, all Profiler data points within a neighborhood of 1 m from each consecutive EM38 data point were averaged. Despite this, a significant correlation ($R^2 = 0.5$) between the two data sets exists, whereby the RMSE is relatively low with 2.14 mS m^{-1} (Fig. 8). As indicated by the regression, the Profiler data tend to slightly overestimate the EM38 data. This can be explained by the difference in coil separation (1.22 m for the Profiler and 1 m for the EM38) leading to a slightly deeper sensitivity of the Profiler. In addition, support scales and measurement spacings were different.

A linear mixed model (Eq. (5)) was used to evaluate the effects of tillage, sensor, and sensor operating frequency on ECa. The sensor and frequency effects as well as the interaction between sensor and frequency were all significant (p b 0.0001), while the tillage effect, the interaction between sensor and tillage, the interaction between frequency and tillage, and the triple interaction were not significant (p = 0.1387, p = 0.1581, p = 0.9738, and p = 0.9957, respectively). This confirms

Published in : Journal (année), vol. xx, n°xx, pp. xx–xx
DOI:xxxxxxxxxxxxxxx
Status : Postprint (Author's version)

the observations made from Fig. 7 that tillage has no significant impact on the bulk soil electrical conductivity within the root zone, which is probably due to the fact that the EMI sensors used were mainly sensitive to deeper soil layers rather than to the tillage zones.

To analyze the spatial variability of the EC_a measured by the EMI sensors, we computed the corresponding semivariograms using a lag distance of 5 m. Exponential models accounting for a nugget effect were fitted for all the variograms. Fig. 9 shows the variograms of EC_a data obtained by the Profiler at the different operating frequencies and dipole orientations. However, all tillage treatment data were considered in each variogram since no significant tillage effect on ECa was observed. A similar variogram was obtained for the data collected by the EM38 (not shown). It can be seen in Fig. 9 that all the variograms rise over distance and never level off, which results in an effective range larger than the field size (165–252 m). The nugget effect and the sill are significantly larger when operating the Profiler in the vertical mode (3.6–4.3 $(mS\ m^{-1})^2$ and 14.0–15.7 $(mS\ m^{-1})^2$, respectively) compared to the horizontal mode (0.57–0.85 $(mS\ m^{-1})^2$ and 5.2–6.3 $(mS\ m^{-1})^2$, respectively), while only slight differences were observed between the operating frequencies. The nugget/sill ratio is between 23.0 and 29.6% for the vertical mode and between 11.0 and 14.5% for the horizontal mode, which indicates a relatively strong spatial dependence, in particular with the horizontal mode, i.e., in the upper horizons (Cambardella et al., 1994). This spatial correlation is to be attributed to the relatively smooth variations of soil texture and water content within the field.

Fig. 6. *Time-domain representation (b-scan) of the amplitude of the reflected signal measured by the on-ground GPR on a 30 m transect for each tillage system: (a) conventional tillage, (b) deep loosening tillage, and (c) reduced tillage. IS indicates Tx–Rx coupling and coupling with the soil surface. I1 and I2 indicate reflections at the interface between two distinct soil layers.*

Published in : Journal (année), vol. xx, n°xx, pp. xx–xx
DOI:xxxxxxxxxxxxxx
Status : Postprint (Author's version)

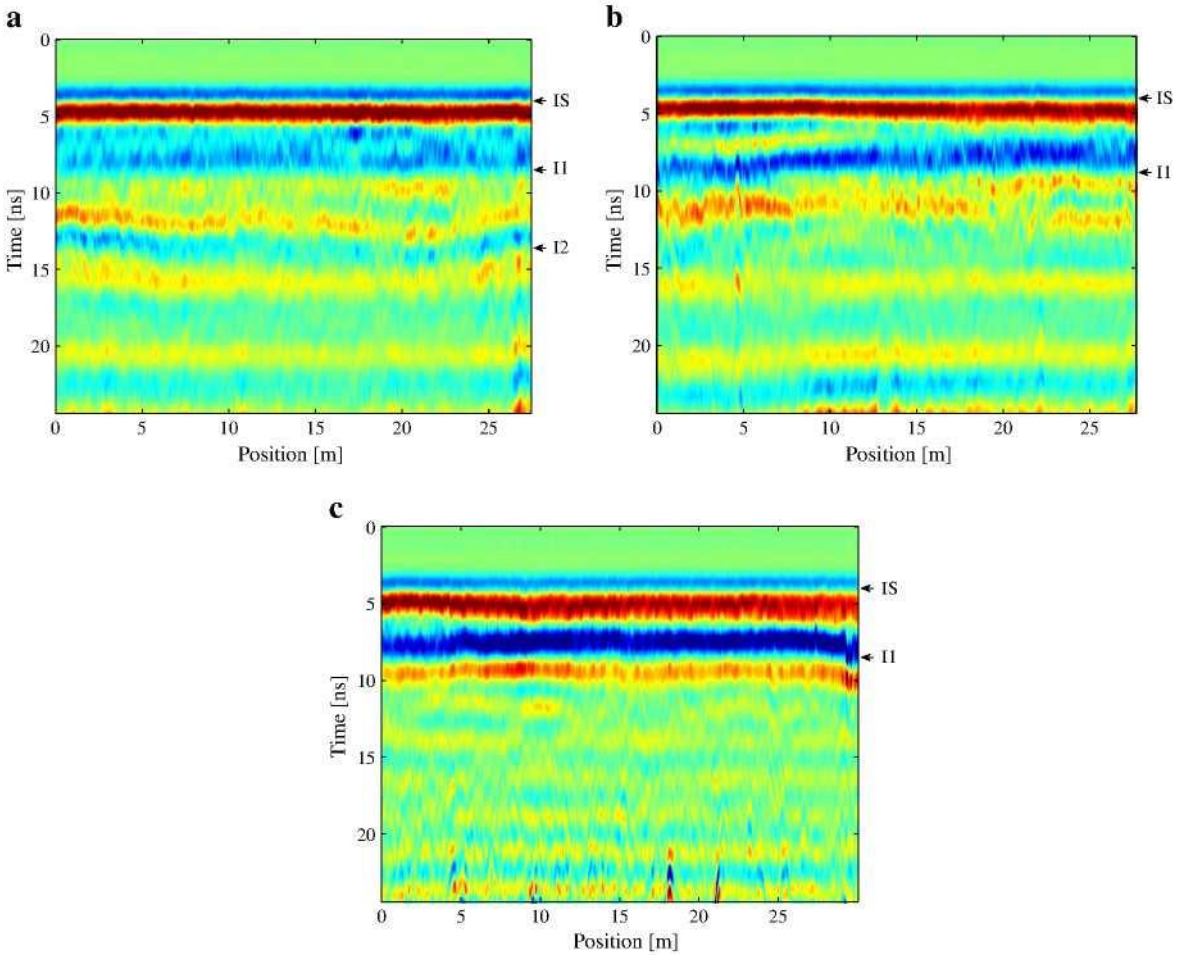

Fig. 7. *Maps of the apparent soil electrical conductivity retrieved by the Profiler using (a) horizontal dipoles (15 kHz), and (b) vertical dipoles (15 kHz), and (c) by the EM38 using vertical dipoles (14.7 kHz) at the Gentinnes study site (April 13, 2010). The tillage treatment applied (CT, DL, and RT) is shown at the bottom-right corner of each plot.*

Published in : Journal (année), vol. xx, n°xx, pp. xx–xx
DOI:xxxxxxxxxxxxxxx
Status : Postprint (Author's version)

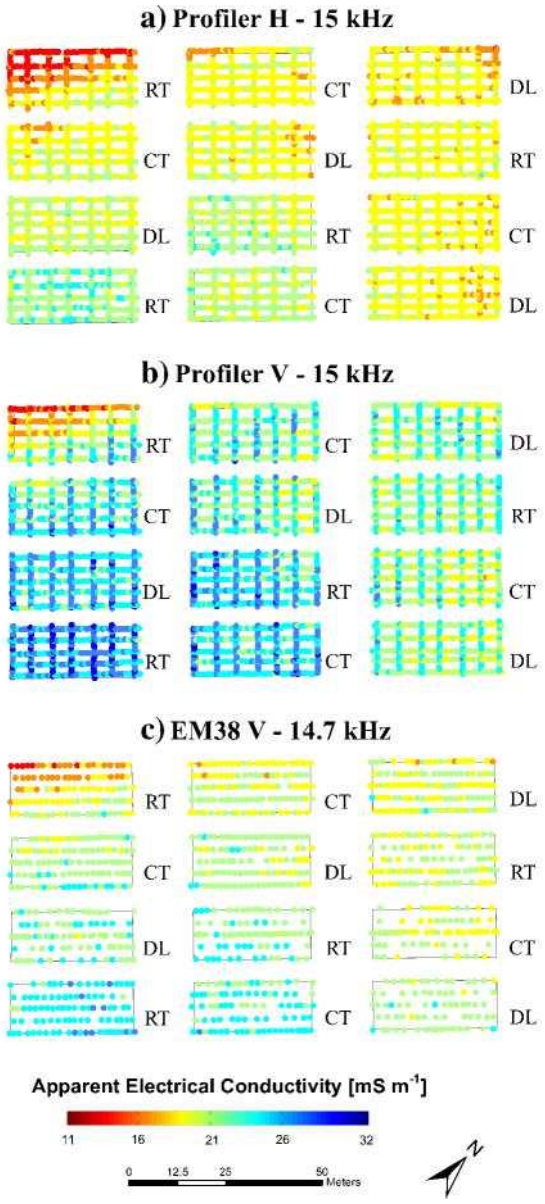

Fig. 8. *Apparent soil electrical conductivity (σ) from EM38 (14.7 kHz, vertical dipoles) versus Profiler (15 kHz, vertical dipoles).*

Published in : Journal (année), vol. xx, n°xx, pp. xx–xx
DOI:xxxxxxxxxxxxxxx
Status : Postprint (Author's version)

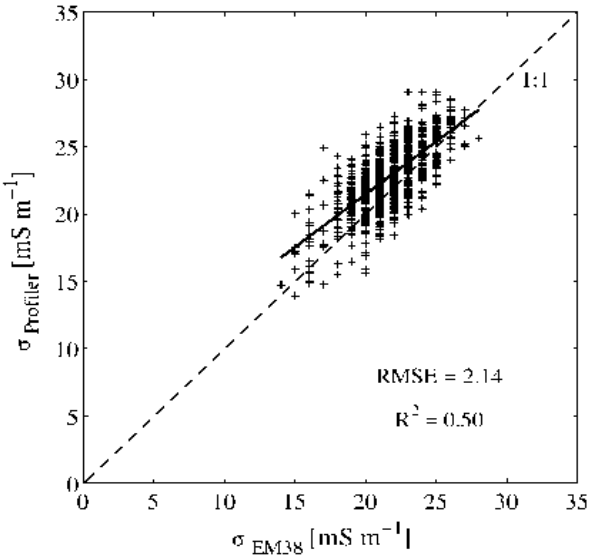

3.3. ROOT ZONE WATER CONTENT

Fig. 10 depicts the gravimetric SWC profiles obtained for each plot. Soil samples were collected at every 5 cm from the surface to a depth of 75 cm at two locations in each plot. Gravimetric water content instead of volumetric water content was measured for these profiles since some uncertainties arose in the estimation of the sample volumes. The gravimetric water content profiles obtained within the plots characterized by CT show the same trends (Fig. 10a). In particular, the profiles show a sharp increase in the water content between the surface and 10–15 cm depth. The water content then decreases up to a depth of 30 cm. Below this depth, water content is relatively constant. The water content profiles observed within the plots characterized by DL show the opposite behavior within the top layers (Fig. 10b) with decreasing values from the surface to 20–30 cm depth. The water content at deeper locations then stays fairly constant. For the RT system, the water content profiles are more heterogeneous (Fig. 10c). In general, water content decreases from the soil surface to 15–25 cm depth and then remains constant below this depth. For all tillage systems, the deep SWC variation range is relatively small and the absolute values are very similar (mean SWC below 40 cm depth is equal to 0.23 g g^{-1} for each tillage system). This confirms that the electrical conductivity variations originate mainly from clay content and not from differences in water content. In addition, SWC in the deeper horizons seems to be unaffected by tillage practices.

Fig. 9. *Semivariograms of the apparent electrical conductivity obtained by the Profiler operating at 15 kHz (red), 10 kHz (blue), and 5 kHz (black) and with vertical (solid lines) and horizontal (dotted lines) dipoles. Each semivariogram was computed using all tillage treatment data with a lag distance of 5 m and fitted with an exponential model.*

Published in : Journal (année), vol. xx, n°xx, pp. xx–xx
DOI:xxxxxxxxxxxxxx
Status : Postprint (Author's version)

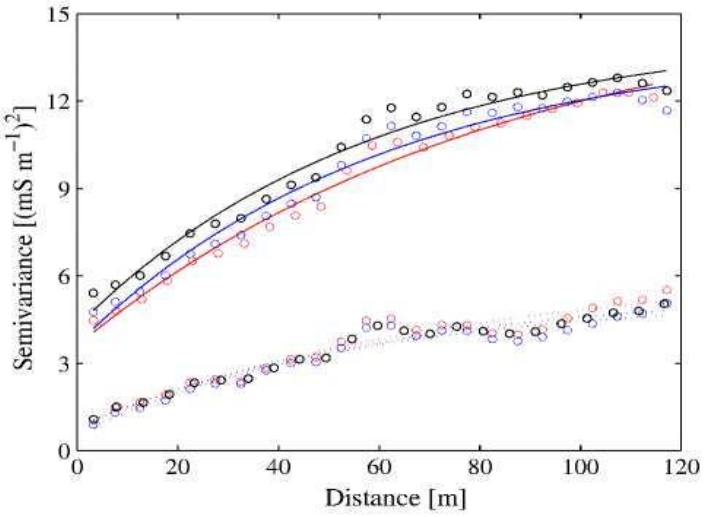

Fig. 10. *Gravimetric soil water content profiles from the surface down to 75 cm depth (5 cm step). Each depicted profile consists of a mean of two measured SWC profiles. Four SWC profiles per tillage system are shown: (a) conventional tillage, (b) deep loosening tillage, and (c) reduced tillage.*

Published in : Journal (année), vol. xx, n°xx, pp. xx–xx
DOI:xxxxxxxxxxxxxx
Status : Postprint (Author's version)

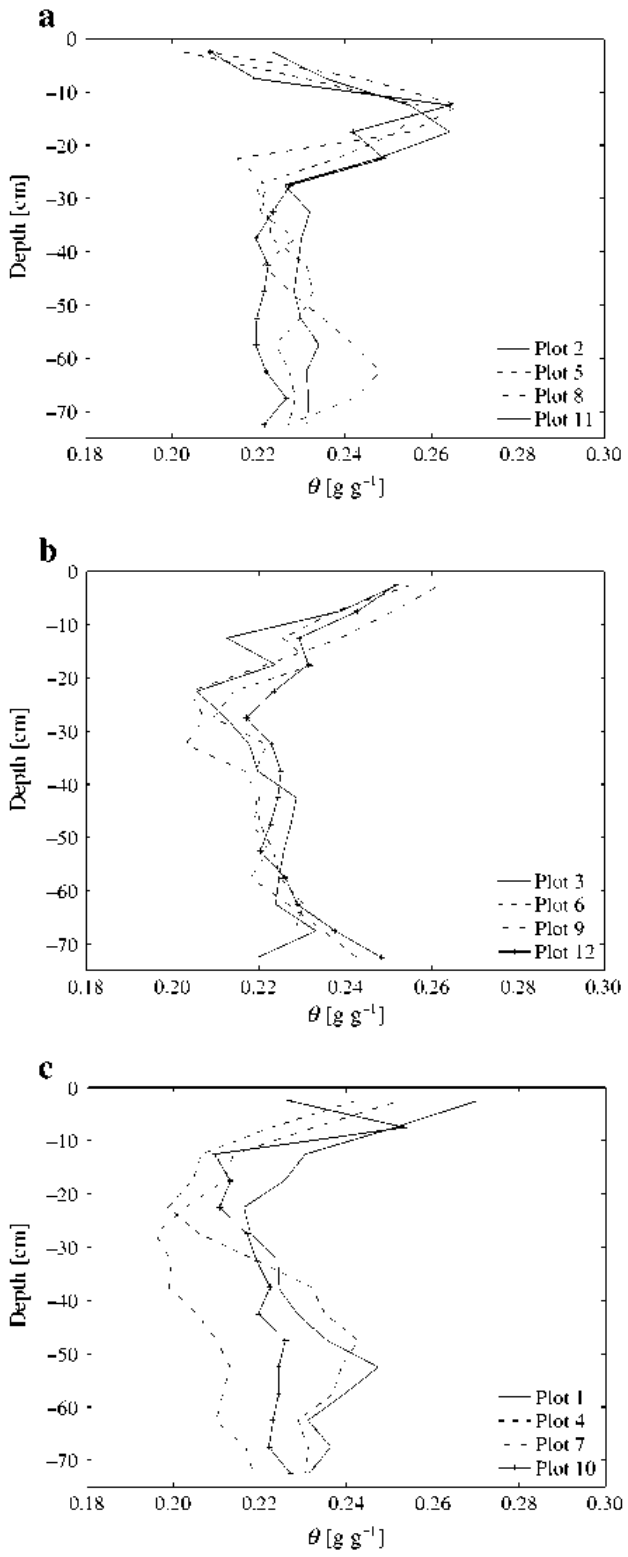

3.4. SURFACE SOIL WATER CONTENT

Fig. 11 presents SWC maps retrieved by (a) volumetric soil sampling, (b) ThetaProbe, (c) 5TE, and (d) off-ground GPR. To allow for a better comparison between the different techniques, all maps have

Published in : Journal (année), vol. xx, n°xx, pp. xx–xx
DOI:xxxxxxxxxxxxxx
Status : Postprint (Author's version)

the same color scale ranging from 0.12 to 0.41 $m^3\ m^{-3}$. In general, all four SWC maps show similar spatial patterns irrespective of the different sensing depths. The SWC map derived from 5TE however shows lower SWC values with a mean of 0.21 $m^3\ m^{-3}$ compared to the mean SWC of 0.27, 0.25, and 0.25 $m^3\ m^{-3}$ for soil sampling, ThetaProbe, and off-ground GPR, respectively. Different numbers of data points were used: 420 measurement points were used for the invasive methods (soil sampling, ThetaProbe, and 5TE) while 927 measurements were collected by the off-ground GPR. Although some trends can be observed, the spatial correlation of surface SWC (see below) is much smaller than for the EMI images (see Section 3.2). This can be attributed to (1) the effect of the shallow tillage practices (see below) and (2) to inherent local heterogeneities. The EMI sensors are less sensitive to local heterogeneities due to the larger sensing volume (1–3 m^3). In comparison, for GPR, the sampling volume is about 0.1 m^3 (1 m^2 × 5–10 cm depth) and for the invasive techniques, the sampling volume is ≤ 100 cm^3.

For a direct comparison of the results obtained from the different measurement methods, off-ground GPR-derived water content is plotted versus water content derived from ThetaProbe, 5TE, and volumetric soil sampling (Fig. 12). As the GPR measurements were continuously performed at predefined transects with high density, all GPR data points within a neighborhood of 1 m from the invasive measurement points were averaged. In general, GPR-derived water contents are much better correlated to the sensor-derived water contents θThetaProbe (R^2 = 0.31, RMSE = 0.040 $m^3\ m^{-3}$) and θ5TE (R^2 = 0.39, RMSE = 0.045 $m^3\ m^{-3}$) than to the soil sampling ($\theta_{Sampling}$) data (R^2 = 0.10, RMSE = 0.060 $m^3\ m^{-3}$). Not only is the correlation between θGPR and $\theta_{Sampling}$ weak, but also the scattering is high and the regression is far off the 1:1 line. Additionally, the range of SWC values is much smaller for the 5TE sensor (0.14–0.28 $m^3\ m^{-3}$) compared to the other methods, with 0.15–0.34, 0.16–0.41, and 0.13–0.36 $m^3\ m^{-3}$ for the ThetaProbe, soil sampling, and GPR, respectively. However, comparing groundtruth and GPR-derived SWC data is not straightforward as the sampling volumes are not the same. In particular, the sampling volume for GPR depends on the SWC itself. In fact, as the analysis is based on the surface reflection, the permittivity retrieved at the air–soil interface is a surface property, assuming that the volume of influence has the same property (Lambot et al., 2006). Heterogeneities near the soil surface (e.g., shallow layering) can indeed lead to constructive or destructive interferences and affect permittivity estimates (Minet et al., 2010). Soil electrical conductivity can also affect the signal reflection at the air–soil interface. However, according to Lambot et al. (2006), the effect can be neglected for conductivity values below 30 mS m^{-1} for the operating frequency range, which is the maximum value observed in the field.

The intention of using three different ground-truth measurement techniques was to provide insights into the effect of the sensor-specific measurement volume and/or measurement accuracy. Therefore, we also analyzed the correlation between the sensors (Fig. 13). The correlation between $\Theta_{Thetaprobe}$ and $\Theta_{Sampling}$ is relatively weak with an R^2 of 0.24, and the correlation between Θ_{5TE} and $\Theta_{Sampling}$ is also weak with an R^2 of 0.13. Additionally, both correlations are far off the 1:1 line with a slope of 0.35 for the $\Theta_{Thetaprobe}$ and $\Theta_{Sampling}$, and 0.19 for the $\Theta_{Thetaprobe}$ and $\Theta_{Sampling}$ relationship. In contrast, correlation between Θ_{5TE} and $\Theta_{Thetaprobe}$ shows fairly good agreement with an R^2 of 0.50 (RMSE = 0.046) and only a parallel shift to the 1:1 line indicating a systematic overestimation of the ThetaProbe data. The differences between the three methods can be partly explained by the

Published in : Journal (année), vol. xx, n°xx, pp. xx–xx
DOI:xxxxxxxxxxxxxxx
Status : Postprint (Author's version)

different sensing volumes (100 cm^3 for the soil sampling, ≈ 75 cm^3 for the ThetaProbe, and ≈ 50 cm^3 for the 5TE sensor) as well as differences in the sensing depths with 5, 6, and 5.2 cm for the soil sampling, ThetaProbe, and 5TE sensor, respectively. Nevertheless, it is still questionable why the method of integrating over the largest volume (namely, soil sampling) deviates so much from the sensor-based data (Fig. 13a). On the other hand, it now seems logical that the correlation between θ_{GPR} and $\Theta_{Sampling}$ is also weak (Fig. 12c), because the soil samples do show a clear difference compared to the sensor-based data.

Fig. 11. *Soil water content maps obtained using (a) volumetric soil sampling, (b) ThetaProbe capacitance sensor, (c) 5TE capacitance sensor, and (d) off-ground GPR at the Gentinnes study site (April 13, 2010). The tillage treatment applied (CT, DL, and RT) is shown at the bottom-right corner of each plot.*

Published in : Journal (année), vol. xx, n°xx, pp. xx–xx
DOI:xxxxxxxxxxxxxxx
Status : Postprint (Author's version)

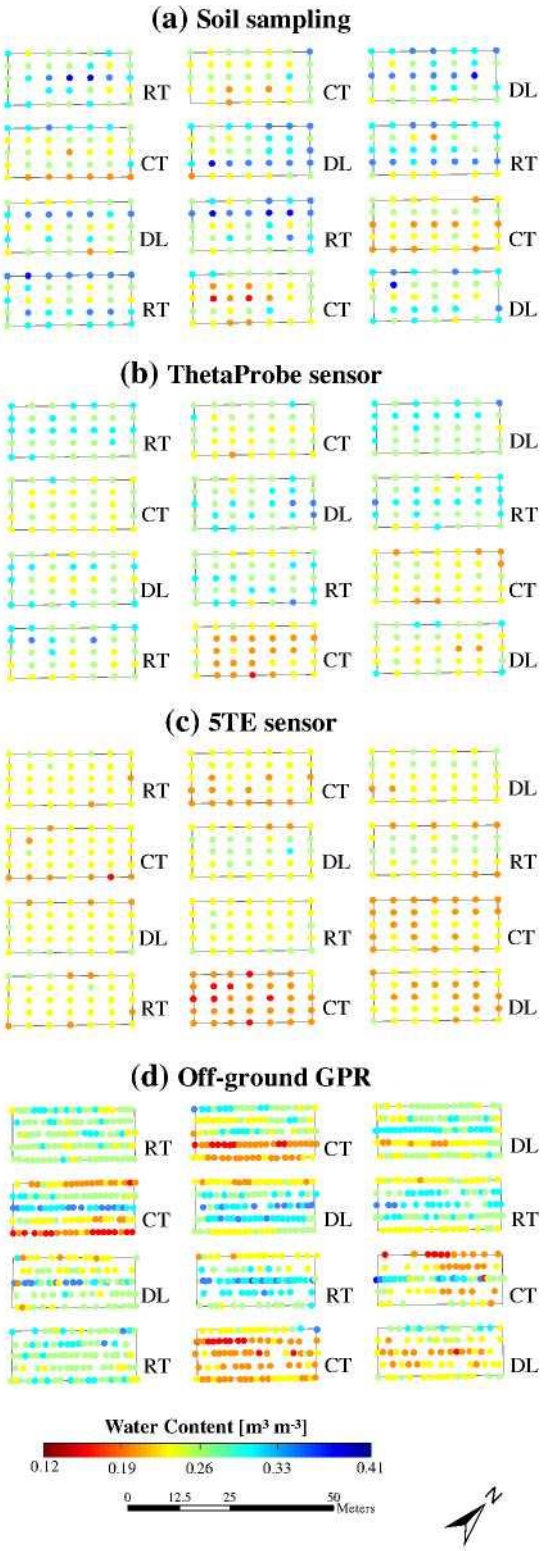

Fig. 12. *Volumetric soil water content from (a) the ThetaProbe capacitance sensor, (b) the 5TE capacitance sensor, and (c) volumetric soil sampling versus off-ground GPR. For the GPR and the two*

Published in : Journal (année), vol. xx, n°xx, pp. xx–xx
DOI:xxxxxxxxxxxxxx
Status : Postprint (Author's version)

capacitance sensors, water content estimates were derived from the dielectric permittivity measurements using Topp's model.

Published in : Journal (année), vol. xx, n°xx, pp. xx–xx
DOI:xxxxxxxxxxxxxxx
Status : Postprint (Author's version)

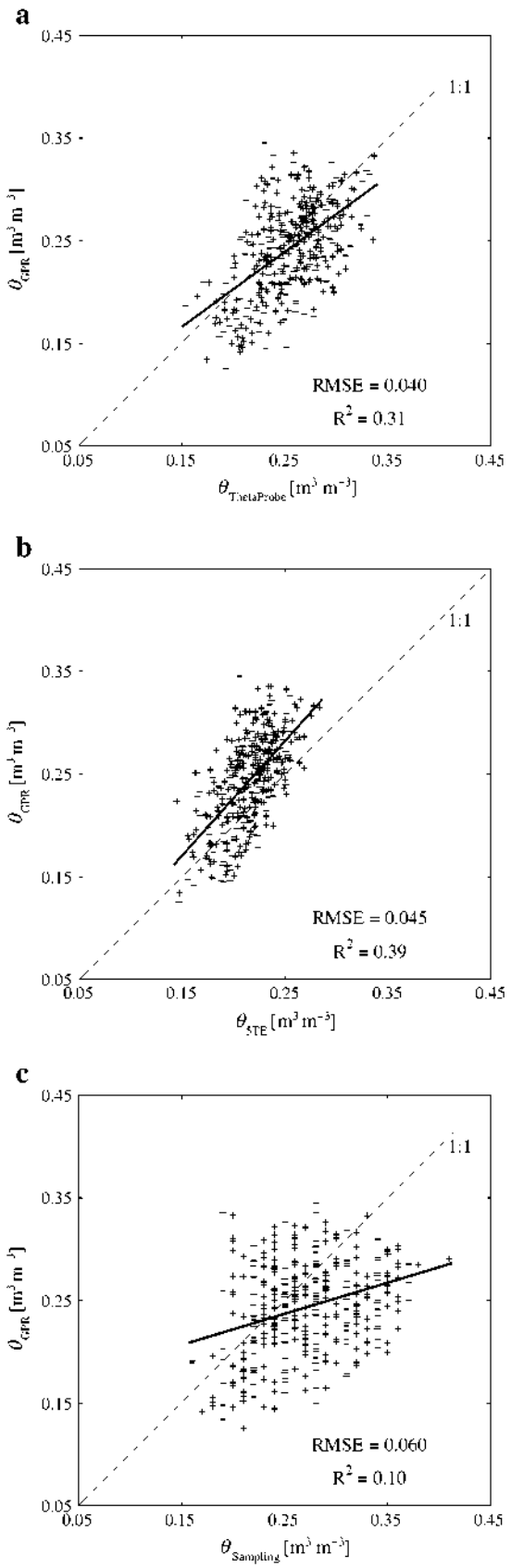

Published in : Journal (année), vol. xx, n°xx, pp. xx–xx
DOI:xxxxxxxxxxxxxx
Status : Postprint (Author's version)

Fig. 13. *Volumetric soil water content from (a) volumetric soil sampling versus ThetaProbe and 5TE capacitance sensors and (b) the 5TE capacitance sensor versus the ThetaProbe capacitance sensor. For the two capacitance sensors, water content estimates were derived from the dielectric permittivity measurements using Topp's model.*

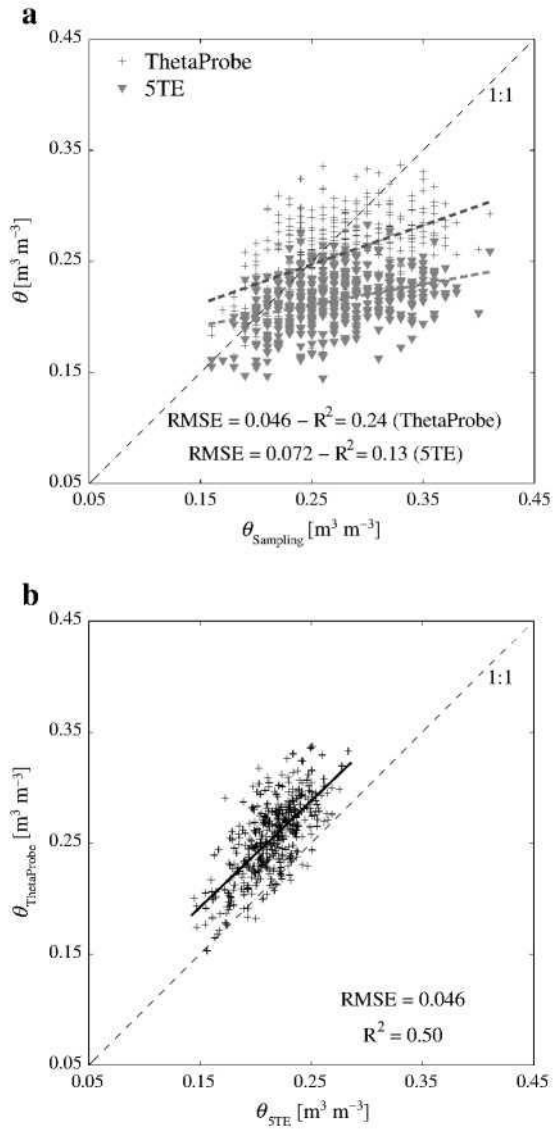

3.5. TILLAGE EFFECT ON SURFACE SOIL WATER CONTENT

To get a better insight into the tillage effect on surface SWC measured by the different sensing techniques, a linear mixed model was used (Eq. (4)). The three fixed effects of the model, i.e., the sensor effect, the tillage effect, and the interaction between sensor and tillage were all significant (p b 0.0001, p b 0.0001, and p = 0.0098, respectively). In Fig. 14, the mean SWC per tillage for each sensing technique and the associated confidence interval (α = 0.05) were determined based on the fitting of the linear mixed model (Eq. (4)). A significantly lower mean SWC is observed in the CT plots compared to all other plots, irrespective of the measurement techniques used (p ≤ 0.0003), whereby

Published in : Journal (année), vol. xx, n°xx, pp. xx–xx
DOI:xxxxxxxxxxxxxxx
Status : Postprint (Author's version)

the 5TE data generally indicate the lowest mean water contents and the soil sampling data indicate the largest. In between are the ThetaProbe and the off-ground GPR data with comparable results as already pointed out above. This lower mean water content in the CT plots can be partly explained by lower pore connectivity between the topsoil and the deeper layers after plowing, which reduces capillary upward water flow from the deeper, wetter layers. This is in agreement with the findings of Mahboubi et al. (1993) and Kosutic et al. (2001), who observed a higher soil water retention with no tillage treatment compared with CT treatment. On the other hand, DL and RT show no significant difference in surface SWC with the three invasive methods and the off-ground GPR system, which indicates a comparable evaporation loss and/or infiltration capacity.

In the next step, we plotted the mean SWC of each plot for all sensors versus the standard deviation (STD) of the measurements (Fig. 15). In general, the STD increases with increasing mean SWC in the observed range of variation. This general trend is in good agreement with the observations of Ryu and Famiglietti (2005) and Choi and Jacobs (2007), who showed that the spatial variability of SWC increases from very dry to wet conditions, reaches a maximum at specific water contents, and then decreases with further wetting until saturation. Vereecken et al. (2007) found that the soil hydraulic properties themselves control the shape of this curve and the point where the maximum will occur. Unfortunately, the SWC values observed are probably below the critical value (maximum STD point) described by the authors, and therefore, a detailed analysis of the differences in soil hydraulic properties due to the tillage systems is restricted. Nevertheless, each tillage system shows a distinct shape of the curve (Fig. 15), which could suggest different hydraulic properties and/or different spatial variabilities of water content within the surface layer.

Finally, we analyzed the spatial variability of the surface SWC obtained by off-ground GPR for the different tillage systems. Among the SWC data sets available in this study, we chose the GPR data set, mainly because this sensor had a larger number of acquisition points and the largest support scale, resulting in the largest coverage rate among all the sensors used in this study (Jonard et al., 2011; Lambot et al., 2006; Minet et al., 2012). Therefore, the GPR could better capture the SWC variability at the plot scale. Semivariograms were computed using GPR-derived SWC estimates from clusters of plots characterized by the same tillage system. The resulting variograms are depicted in Fig. 16 for CT, DL, and RT. Each variogram was computed with a lag distance of 5 m and fitted with an exponential model. The GPR data were not evenly distributed but clustered in non-contiguous plots, which may explain the undulating effect observed in the variograms. In general, the quality of the fit is reasonable with an R^2 between 0.54 and 0.62. These graphs reveal the distinct spatial behavior of the SWC within the three tillage systems.

Fig. 14. *Mean soil water content per tillage (conventional tillage, deep loosening tillage, and reduced tillage) for each measurement technique $\hat{\vartheta}_T\hat{}$. Error bars represent the confidence intervals ($\alpha = 0.05$) and colors represent the measurement techniques (red: volumetric soil sampling, green: ThetaProbe capacitance sensor, black: 5TE capacitance sensor, and blue: off-ground GPR).*

Published in : Journal (année), vol. xx, n°xx, pp. xx–xx
DOI:xxxxxxxxxxxxxx
Status : Postprint (Author's version)

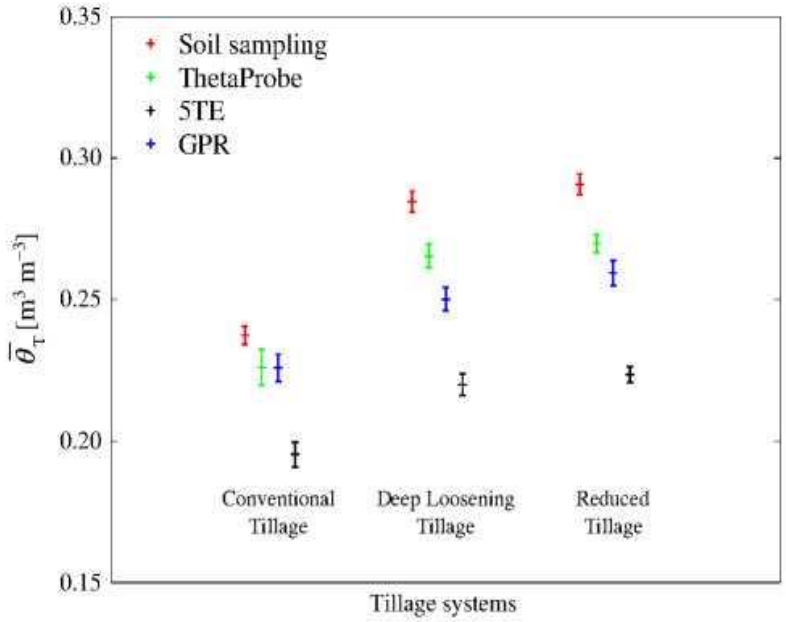

Fig. 15. *Soil water content standard deviation, STD ϑ, with respect to mean soil water content per plot, ϑP, obtained from measurements made using volumetric soil sampling (circles), ThetaProbe capacitance sensor (squares), 5TE capacitance sensor (triangle), and off-ground GPR (filled triangles) at the Gentinnes study site (April 13, 2010). Colors represent tillage systems (red: conventional tillage, blue: deep loosening tillage, and green: reduced tillage). Dashed lines represent linear regression lines for each tillage system. (For interpretation of the references to color in this figure legend, the reader is referred to the web version of this article.)*

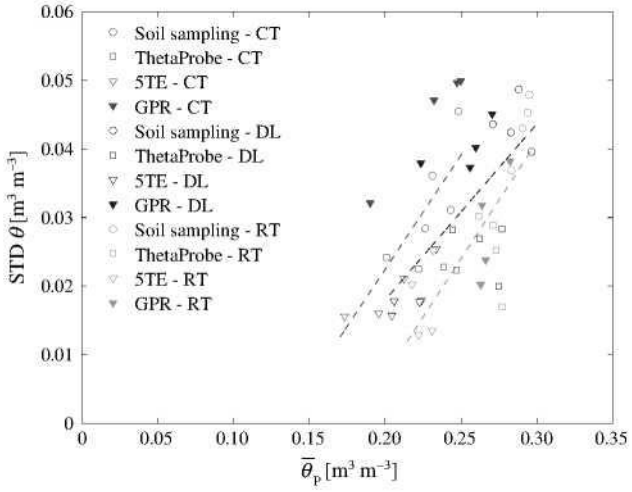

Fig. 16. *Semivariograms of off-ground GPR-derived soil water content computed for the plots prepared with conventional tillage (red), deep loosening tillage (blue), and reduced tillage (black). Each semivariogram was computed with a lag distance of 5 m and fitted with an exponential model.*

Published in : Journal (année), vol. xx, n°xx, pp. xx–xx
DOI:xxxxxxxxxxxxxx
Status : Postprint (Author's version)

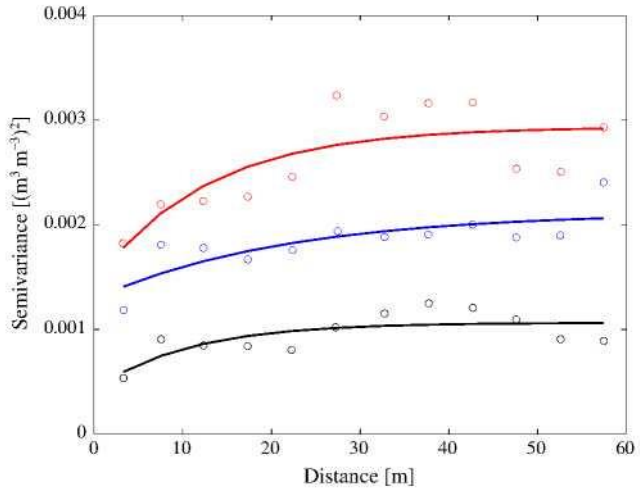

Table 1. *Semivariogram parameters of off-ground GPR-derived SWC computed for the plots prepared with conventional tillage, deep loosening tillage, and reduced tillage.*

	Nugget [$(m^3\ m^{-3})^2$]	Sill [$(m^3\ m^{-3})^2$]	Nugget/sill [%]	Effective range [m]	R^2
Conventional tillage	0.00144	0.00294	49	38	0.62
Deep loosening tillage	0.00129	0.00212	61	65	0.61
Reduced tillage	0.00042	0.00106	40	32	0.54

The variogram parameters are shown in Table 1. The nugget effect, which can be attributed to measurement errors and/or spatial sources of variation at distances smaller than the shortest sampling interval, is significantly smaller for RT compared to the other two tillage treatments. For each variogram, the effective range is larger than the plot size (>30 m). The DL variogram is characterized by a large range (65 m) and a high nugget/sill ratio (61%), which suggests a rather random and unstructured spatial variability. Conversely, the nugget/ sill ratio is smaller for CT and RT (49 and 40%, respectively), which indicates a clear spatial autocorrelation, even though they are characterized by a shorter range (38 and 32 m, respectively). The larger sill of the CT variogram indicates that the variance of the SWC within the CT plots is larger than within the other plots. This larger SWC variability could be explained by a larger soil heterogeneity induced by the plowing process. Indeed, using a moldboard plow, soil blocks from deeper layers characterized by higher bulk densities (in general, the soil bulk density increases with depth) are locally transferred to the surface, and therefore, increase the variability in SWC. Additionally, the plowing also creates local compaction which modifies the SWC distribution. An intermediate sill value is observed for DL which could be explained by lower soil mixing compared to CT (especially between the tines), but higher soil mixing compared to RT (along the path of the tines).

Published in : Journal (année), vol. xx, n°xx, pp. xx–xx
DOI:xxxxxxxxxxxxxxx
Status : Postprint (Author's version)

4. Summary and conclusion

In this study, we used geophysical methods to analyze the effects of tillage on surface soil water content, bulk soil electrical conductivity, and mechanical resistance. GPR and EMI data were collected on three contrasting tillage practices applied to an agricultural field: (1) conventional tillage, (2) deep loosening tillage, and (3) reduced tillage. As additional measurements, soil sampling, capacitance probe, and soil penetrometer data were acquired as ground truths. The data showed that tillage influences the soil resistance (deeper tillage decreases soil resistance), which could be partly seen in on-ground GPR data. We also observed a tillage effect on shallow surface SWC, while deeper SWC seems to be unaffected by tillage. Mean surface SWC was significantly lower for CT compared to DL and RT. This was partly explained by lower pore connectivity between the topsoil and the deeper layers after conventional tillage, which reduces capillary upward water flow from the deeper, wetter layers. The variance of the SWC within the conventional tillage plots was larger than within the other plots. This larger SWC variability could be explained by a soil heterogeneity induced by the plowing process. This study confirms the potential of GPR and EMI sensors for the determination of soil physical properties at field scale and for the characterization of agricultural management practices. These geophysical techniques could also help us to apply precision agricultural practices for efficient resource management and crop yield enhancement.

Acknowledgments

This research was supported by the German Research Foundation (DFG) in the framework of the Transregional Collaborative Research Centre 32 and Fonds de la Recherche Scientifique (FNRS, Belgium).

We would like to extend our gratitude to the Walloon Agricultural Research Centre (Agriculture and Natural Environment Department) for the preparation of the experimental plots and its support during the field campaign.

References

Alletto, L., Coquet, Y., Justes, E., 2011. Effects of tillage and fallow period management on soil physical behaviour and maize development. Agricultural Water Management 102 (1), 74–85.

André, F., van Leeuwen, C., Saussez, S., Van Durmen, R., Bogaert, P., Moghadas, D., de Resseguier, L., Delvaux, B., Vereecken, H., Lambot, S., 2012. High-resolution imaging of a vineyard in south of France using ground-penetrating radar, electromagnetic induction and electrical resistivity tomography. Journal of Applied Geophysics 78 (0), 113–122.

Basso, B., Amato, M., Bitella, G., Rossi, R., Kravchenko, A., Sartori, L., Carvahlo, L.M., Gomes, J., 2011. Two-dimensional spatial and temporal variation of soil physical properties in tillage systems using electrical resistivity tomography. Agronomy Journal 102 (2), 440–449.

Brosten, T.R., Day-Lewis, F.D., Schultz, G.M., Curtis, G.P., Lane, J.W., 2011. Inversion of multi-frequency electromagnetic induction data for 3D characterization of hydraulic conductivity. Journal of Applied Geophysics 73 (4), 323–335.

Brown, H., Prescott, R., 2006. Applied Mixed Models in Medicine, 2nd edition. John Wiley and Sons, New York, USA.

Cambardella, C.A., Moorman, T.B., Novak, J.M., Parkin, T.B., Karlen, D.L., Turco, R.F., Konopka, A.E., 1994. Field-scale variability of soil properties in central Iowa soils. Soil Science Society of America Journal 58 (5), 1501–1511.

Choi, M., Jacobs, J.M., 2007. Soil moisture variability of root zone profiles within SMEX02 remote sensing footprints. Advances in Water Resources 30 (4), 883–896.

Cockx, L., Van Meirvenne, M., De Vos, B., 2007. Using the EM38DD soil sensor to delineate clay lenses in a sandy forest soil. Soil Science Society of America Journal 71 (4), 1314–1322.

Corwin, D.L., Lesch, S.M., 2005. Apparent soil electrical conductivity measurements in agriculture. Computers and Electronics in Agriculture 46 (1–3), 11–43.

Elliott, J.A., Cessna, A.J., Nicholaichuk, W., Tollefson, L.C., 2000. Leaching rates and preferential flow of selected herbicides through tilled and untilled soil. Journal of Environmental Quality 29 (5), 1650–1656.

Friedman, S.P., 2005. Soil properties influencing apparent electrical conductivity: a review. Computers and Electronics in Agriculture 46 (1–3), 45–70.

Huisman, J.A., Hubbard, S.S., Redman, J.D., Annan, A.P., 2003. Measuring soil water content with ground penetrating radar: a review. Vadose Zone Journal 2, 476–491.

Jabro, J.D., Sainju, U.M., Stevens, W.B., Lenssen, A.W., Evans, R.G., 2009. Long-term tillage influences on soil physical properties under dryland conditions in northeastern Montana. Archives of Agronomy and Soil Science 55 (6), 633–640.

Jonard, F., Weihermüller, L., Jadoon, K.Z., Schwank, M., Vereecken, H., Lambot, S., 2011. Mapping field-scale soil moisture with L-band radiometer and ground-penetrating radar over bare soil. IEEE Transactions on Geoscience and Remote Sensing 49 (8), 2863–2875.

Jonard, F., Weihermüller, L., Vereecken, H., Lambot, S., 2012. Accounting for soil surface roughness in the inversion of ultrawideband off-ground GPR signal for soil moisture retrieval. Geophysics 77 (1), H1–H7.

Kosutic, S., Husnjak, S., Filipovic, D., Bogunovic, M., 2001. Influence of different tillage systems on soil water availability in the Ap-horizon of an Albic Luvisol and yield in north-west Slavonia, Croatia. Bodenkultur 52 (3), 215–223.

Kovar, J.L., Barber, S.A., Kladivko, E.J., Griffith, D.R., 1992. Characterization of soiltemperature, water-content, and maize root distribution in 2 tillage systems. Soil and Tillage Research 24 (1), 11–27.

Kulasekera, P.B., Parkin, G.W., von Bertoldi, P., 2011. Using soil water content sensors to characterize tillage effects on preferential flow. Vadose Zone Journal 10 (2), 683–696.

Lambot, S., Slob, E.C., van den Bosch, I., Stockbroeckx, B., Vanclooster, M., 2004. Modeling of ground-penetrating radar for accurate characterization of subsurface electric properties. IEEE Transactions on Geoscience and Remote Sensing 42, 2555–2568.

Lambot, S., Weihermüller, L., Huisman, J.A., Vereecken, H., Vanclooster, M., Slob, E.C., 2006. Analysis of air-launched ground-penetrating radar techniques to measure the soil surface water content. Water Resources Research 42, W11403 (11410.11029/12006WR005097).

Lambot, S., Binley, A., Slob, E., Hubbard, S., 2008. Ground penetrating radar in hydrogeophysics. Vadose Zone Journal 7 (1), 137–139. http://dx.doi.org/10.2136/ vzj2007.0180.

Mahboubi, A.A., Lal, R., Faussey, N.R., 1993. 28 years of tillage effects on 2 soils in Ohio. Soil Science Society of America Journal 57 (2), 506–512.

McNeill, J.D., 1980. Electromagnetic terrain conductivity measurement at low induction numbers. Technical Note TN-6.Geonics Limited, Ontario.

Mester, A., van der Kruk, J., Zimmermann, E., Vereecken, H., 2011. Quantitative two- layer conductivity inversion of multi-configuration electromagnetic induction measurements. Vadose Zone Journal 10 (4), 1319–1330.

Michalski, K.A., Mosig, J.R., 1997. Multilayered media Green's functions in integral equation formulations. IEEE Transactions on Antennas and Propagation 45 (3), 508–519.

Minet, J., Lambot, S., Slob, E.C., Vanclooster, M., 2010. Soil surface water content estimation by full-waveform GPR signal inversion in the presence of thin layers. IEEE Transactions on Geoscience and Remote Sensing 48 (3), 1138–1150.

Minet, J., Bogaert, P., Vanclooster, M., Lambot, S., 2012. Validation of ground penetrating radar full-waveform inversion for field scale soil moisture mapping. Journal of Hydrology 424–425, 112–123.

Müller, M., Kurz, G., Yaramanci, U., 2009. Influence of tillage methods on soil water content and geophysical properties. Near Surface Geophysics 7 (1), 27–36.

Ndiaye, B., Molenat, J., Hallaire, V., Gascuel, C., Hamon, Y., 2007. Effects of agricultural practices on hydraulic properties and water movement in soils in Brittany (France). Soil and Tillage Research 93 (2), 251–263.

Oleschko, K., Korvin, G., Munoz, A., Velazquez, J., Miranda, M.E., Carreon, D., Flores, L., Martinez, M., Velasquez-Valle, M., Brambila, F., Parrot, J.F., Ronquillo, G., 2008. Mapping soil fractal dimension in agricultural fields with GPR. Nonlinear Processes in Geophysics 15 (5), 711–725.

Reedy, R.C., Scanlon, B.R., 2003. Soil water content monitoring using electromagnetic induction. Journal of Geotechnical and Geoenvironmental Engineering 129 (11), 1028–1039.

Richard, G., Rouveure, R., Chanzy, A., Faure, P., Chanet, M., Marionneau, A., Regnier, P., Duval, Y., 2010. Using proximal sensors to continuously monitor agricultural soil physical conditions for tillage management. Proximal Soil Sensing. Progress in Soil Science. Springer, Dordrecht, pp. 313–321.

Roisin, C.J.C., 2007. A multifractal approach for assessing the structural state of tilled soils. Soil Science Society of America Journal 71 (1), 15–25.

Ryu, D., Famiglietti, J.S., 2005. Characterization of footprint-scale surface soil moisture variability using Gaussian and beta distribution functions during the Southern Great Plains 1997 (SGP97) hydrology experiment. Water Resources Research 41 (12), 13.

Sauer, T.J., Clothier, B.E., Daniel, T.C., 1990. Surface measurements of the hydraulic- properties of a tilled and untilled soil. Soil and Tillage Research 15 (4), 359–369.

Schwen, A., Bodner, G., Loiskandl, W., 2011a. Time-variable soil hydraulic properties in near-surface soil water simulations for different tillage methods. Agricultural Water Management 99 (1), 42–50.

Schwen, A., Bodner, G., Scholl, P., Buchan, G.D., Loiskandl, W., 2011b. Temporal dynamics of soil hydraulic properties and the water-conducting porosity under different tillage. Soil and Tillage Research 113 (2), 89–98.

Slob, E., Sato, M., Olhoeft, G., 2010. Surface and borehole ground-penetrating-radar developments. Geophysics 75 (5), A103–A120.

Strudley, M.W., Green, T.R., Ascough, J.C., 2008. Tillage effects on soil hydraulic properties in space and time: state of the science. Soil and Tillage Research 99 (1), 4–48.

Tan, C.S., Drury, C.F., Gaynor, J.D., Welacky, T.W., Reynolds, W.D., 2002. Effect of tillage and water table control on evapotranspiration, surface runoff, tile drainage and soil water content under maize on a clay loam soil. Agricultural Water Management 54 (3), 173–188.

Topp, G., Davis, J.L., Annan, A.P., 1980. Electromagnetic determination of soil water content: measurements in coaxial transmission lines. Water Resources Research 16, 574–582.

Vereecken, H., Kamai, T., Harter, T., Kasteel, R., Hopmans, J., Vanderborght, J., 2007. Explaining soil moisture variability as a function of mean soil moisture: a stochastic unsaturated flow perspective. Geophysical Research Letters 34 (22), 6.

Zhang, S.L., Li, P.R., Yang, X.Y., Wang, Z.H., Chen, X.P., 2011. Effects of tillage and plastic mulch on soil water, growth and yield of spring-sown maize. Soil and Tillage Research 112 (1), 92–97